RSC Advances

ROYAL SOCIETY OF CHEMISTRY

www.rsc.org/advances

Table of Content

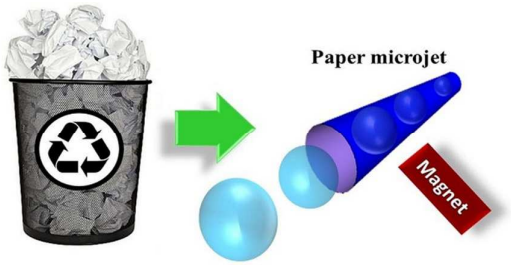

Magneto-catalytic paperbots employing nanoparticle coated waste papers in which the magnetic control was infused by coated of printer ink.

RSC Advances

ARTICLE

Magnetically Guided Chemical Locomotion of Self-Propelling Paperbots

Received 00th January 20xx,
Accepted 00th January 20xx

DOI: 10.1039/x0xx00000x

www.rsc.org/

Amit Kumar Singh,[a] Tapas Kumar Mandal*[ab] and Dipankar Bandyopadhyay*[ab]

Self-propelling microjets with multimodal chemical and magnetic controls on the motion were prepared from the printed waste papers coated with MnO_2 nanoparticles. While the magnetic remote control was infused from the ferromagnetic coating of the printer ink, the nanoparticles decomposed peroxide fuel to induce locomotion by ejecting oxygen bubbles though the microjet. The paper microjets could be loaded with the fluorescent rhodamine 6G (R6G), a model payload, before remotely guided through an external magnetic field inside fluidic environment. The reported methodology provides an economic, scalable, and biodegradable scheme for the design and development of bubble-propelled microengines, which are capable of directed locomotion.

1. Introduction

Synthesis of artificial swimmers of macro, micro or nanoscale dimension has emerged as an active area of research owing to their significant technological importance.[1-8] The synthetic self-propelling objects are expected to perform diverse tasks harnessing different sources of energy for their locomotion which includes the chemical energy,[1,9] surface tension force,[7,10] photonic[11] or acoustic[12-14] or thermal excitations,[15,16] and external electric[17] and magnetic[18] fields, among others. In particular, the minuscule self-propelling tubular microjets[19] are envisioned to serve as the cargo transporters,[20] drug delivery modules,[21] agents for the environmental remediation[8] and building blocks for the lab-on-a-chip devices.[22]

In general, the microjets are fabricated by rolling up the membranes of relatively inert materials such as the titanium, polycarbonate and aluminum oxide coated with active metal films.[23] The rolling is done in such a manner that the inert layer forms the outer shell while the active layers stay inside the hollow core. Interestingly, when the tubular microjets are placed inside a bath of peroxide fuel (dilute hydrogen peroxide – H_2O_2), the active layers catalytically decomposes the H_2O_2 to produce a stream of oxygen (O_2) bubbles from the hollow inner core. The recoiling of the microengine during the ejection of the O_2 bubbles provides the required thrust for the motion. Previous studies suggest that fabrication of the microengines are multistep processes and needs facilities such as template-assisted electrodeposition, electron beam evaporation and photolithography.[23-25] Clearly, a simpler and cost-effective methodology to fabricate the microengines is more preferred option to provide further impetus on the applicability and commercialization of these devices.

In this direction, inspired by the recent research works on the paper-based microfluidics,[26] we report the synthesis of a paper microjet, which shows locomotion under the chemical and magnetic triggers. We employ a simple methodology to fabricate the microengines by rolling up the printed waste papers in which the chemical sensitivity was brought in by depositing MnO_2 nanoparticles on a paper surface. These microengines were inherently sensitive towards external magnetic field because of the presented of the ferromagnetic printer ink on their surface. The target here is to recycle the printed waste papers for the fabrication of the microengines after minor chemical modifications. Arguably, for the first time the results reported in this work highlight the directed propulsion of the paper microjets in combination with the motion triggered by the chemical excitations. Example situations for payload transport were demonstrated where the paper microjets could be loaded with the fluorescent rhodamine 6G (R6G) as model cargo before remotely guided through an external magnetic field inside a fluidic environment. The reported methodology provides a scalable cum biodegradable scheme for the design and development of bubble-propelled microengines, which are capable of directed propulsion through remote guidance.

2. Experimental methods

2.1. Materials and methods

Hydrogen peroxide (H_2O_2) (50%), ethanol (C_2H_6O) (99.9%), fluorescein sodium salt ($C_{20}H_{10}Na_2O_5$) and potassium permanganate ($KMnO_4$), Amberlite IR 120 were obtained from

[a] Centre for Nanotechnology, Indian Institute of Technology Guwahati, Guwahati-781039, India.
[b] Department of Chemical Engineering, Indian Institute of Technology Guwahati, Guwahati -781039, India.
*E-mail: tapasche@iitg.ernet.in,dipban@iitg.ernet.in

Electronic Supplementary Information (ESI) available: Detailed experimental protocol, characterization and movies of motor motion along with detailed explanation. See DOI: 10.1039/x0xx00000x

Merck (India). Rhodamine 6G ($C_{28}H_{31}N_2O_3Cl$) was obtained from Sigma Aldrich, India. The chemicals above were of analytical grade and used without further purification. The water used in all the experiments was of Milli-Q grade. The printer (Model: HP LaserJet Pro P1606dn) and black print cartridge (Product Code: CE278A) were purchased from Hewlett-Packard India. The A4 sized papers (210 mm × 297 mm) were collected from the waste. The adhesive tube (FEVIQUICK®) was obtained from Pidilite Industries Ltd. (India).

2.2. Fabrication of magneto-catalytic paper microjets

The microjet was fabricated using discarded paper sheets from the black and white laser jet printer. The one side of the flat piece of paper was uniformly coated with the toner ink of the printer by taking a printout in black ink, which infused the magnetic sensitivity by depositing ferromagnetic layer of Fe_3O_4 microparticles on the paper surface.[27] Thereafter, the paper was cut into 1 cm × 1 cm square pieces. Following this, the manganese dioxide nanoparticles (MnO_2NPs) were deposited chemically on the non-printed side of the paper. The non-printed side of paper was dipped horizontally into a 0.45 M alkaline $KMnO_4$ ($KMnO_4$: NaOH = 1:1 in molar ratio) in such a way that the $KMnO_4$ makes a thin coating on the paper surface. Then the alkaline $KMnO_4$ coated paper was kept at room temperature for 10 h under a 100 W incandescent light exposure. The color of the paper surface changed from purple to brown due to formation of MnO_2NPs. The product was then washed with water and dried at 60 ^oC for 2 h. The detailed mechanism for formation of MnO_2NPs over cellulose fibers of paper have been previously explained by Wang *et al.*[28] The MnO_2NPs infused the chemical activation of the paper as the MnO_2NPs could catalytically decompose H_2O_2 ($2H_2O_2 \rightarrow 2H_2O + O_2$)[29] when the paper was immersed inside a bath of peroxide fuel. After the deposition of MnO_2NPs, the flat piece of paper was rolled up manually and sealed with adhesive to form a tubular microjet where the toner ink coating stayed outside and the MnO_2NPs stays at the inner hollow core in the range of 300-600 µm. Thereafter, the tubular microjet was cut into pieces with a sharp surgical scissor of varying length ranging from 900 µm to 2 mm. The microjets of size ~900 µm with diameter opening of ~350 µm were used for all the experiments. The microjets were cut randomly and only those were selected for the experiments, which had significant difference in the diameter at the sides. This ensured that the shape of the microjet was similar to the frustum of a cylinder, which was verified through the microscopic inspections. For fabrication of catalytic microjet without the magnetic handle, a non-printed paper of dimension 1 cm × 1 cm was cut before following the steps mentioned previously to coat the MnO_2NPs.

2.3. Fabrication of fluorescent catalytic paper microjets

The fluorescein sodium salt was dissolved in water to obtain 0.1 M solution. The solution was drop casted on the paper microjets and then the catalytic microtubes were dried at 40 ^oC for 2 h. The fluorophore solution stained the cellulose fibers of the paper microjets making it fluorescent.[30] The fluorescence activity is observed at UV excitation of 494 nm. The paper microjet appeared to be green in color.

2.4. Measurement of speed with the variation in the peroxide concentration

A paper microjet (size ~900 µm) was suspended in a petri dish (dia. 4 cm) filled with aqueous H_2O_2 solution. The petri dish was placed on a paper-grid (dimension 1 mm × 1 mm) to measure the displacement.[31] The speed of the microjet was estimated by measuring the displacement of the microjet from starting point to the final position per unit time. The speed of the microjet (V_c) was studied for different concentrations of the peroxide fuel from 10% to 16%. Experiments were performed with five different motors to obtain the mean and the error bars.

2.5. Measurement of speed with the variation in the magnetic field strength

Initially, the paper microjets (size ~900 µm) were suspended in a petri dish filled with 4 mL of 10% (v/v) aqueous H_2O_2 solution. The petri dish was placed on a paper-grid (1 × 1 mm dimension) to measure the displacement.[31] The external magnetic field was applied across the petri dish with the help of an electromagnet and the field strength was varied from 10 – 60 mT. The speed of the motor (V_m) was calculated after every 1 mm displacement of the motor per unit time towards one of the poles of the magnet. Experiments were performed with five different motors to obtain the mean and the error bars.

2.6. Rate constant measurement for H_2O_2 decomposition

The rate of decomposition of H_2O_2 solution by a catalytic paper microjet was analyzed by volumetric titration with $KMnO_4$.[31] The strength of the $KMnO_4$ was standardized by 0.2 N oxalic acid. Firstly, a 5 mL of 10% (v/v) H_2O_2 was taken in a petri dish and then one catalytic microjet (~900 µm size) was immersed in the peroxide bath. After every 2 min time interval, a 200 µL aliquot was withdrawn and added to 8 mL 0.2 N H_2SO_4 solution. Following this, the solution was titrated against standard 0.2 N $KMnO_4$ solutions in which development of permanent faint pink coloration confirmed the end point. The H_2O_2 concentration changed with time as the inner catalytic MnO_2 layer of microjet decomposed the fuel while in motion. The rate constant (k) for the H_2O_2 decomposition was estimated. The straight line with negative slope of the plot confirmed that H_2O_2 decomposition followed first-order kinetics.

2.6. Cargo loading on magnetic paper microjets and directional control

Rhodamine 6G (R6G), a dye representative of cationic drugs such as quinine and procaine, was used as payload for attachment.[32] A magnetic paper microjet (devoid of inner catalytic MnO_2 layer) was placed on a glass slide and 5 ml ethanoic solution of R6G (0.1 g/ml) was drop-casted. Following this, it was kept at 37 ^oC for 2 h for evaporation of ethanol. The evaporation of ethanol resulted in self-assembly and

electrostatic binding of the cargo on outer layer of the paper microjet. The electrostatic interactions between the cationic R6G molecules and anionic toner ink resulted in binding of R6G over the outer magnetic layer. The motor was washed twice to remove unabsorbed R6G. The paper microjet was suspended in water filled petridish and the movement of the motor was remotely controlled with the help of an external permanent magnet. The microjet demonstrated sole magnetic locomotion in this case.

2.7. Equipment

Field emission scanning electron microscopy (Quanta FEG250 and Zeiss Sigma FESEM, Germany) were used to examine the surface of the paper microjets. The surface characterization of paper microjets were further done by X-ray diffraction (XRD, Bruker AXS Advance D8 diffractometer, Cu Kα source, X-ray wavelength 1.54 Å) and Fourier transform infrared (FTIR) spectrometer (Shimadzu, IRAffinity1). The magnetization curve was determined by vibrating sample magnetometer (VSM, Lakeshore GMW magnetic systems 3474-140). The motions of the moving microjets in dilute peroxide fuel were recorded with a Sony Cybershot DSC-HX100V digital camera (Sony Corp., Japan). The florescent activity of paper microjets were observed under the fluorescent mode of Leica DM 2500 upright microscope at 2.5x magnification. The electromagnet Model EMU-50V with constant current power supply unit (DPS – 50) was used to apply the magnetic field in various experiments and the applied magnetic field was measured by Digital Gaussmeter Model DGM-102 (purchased from SES instruments, India).

3. Results and discussion

The microjet was fabricated using discarded paper sheets from the black and white laser jet printer.

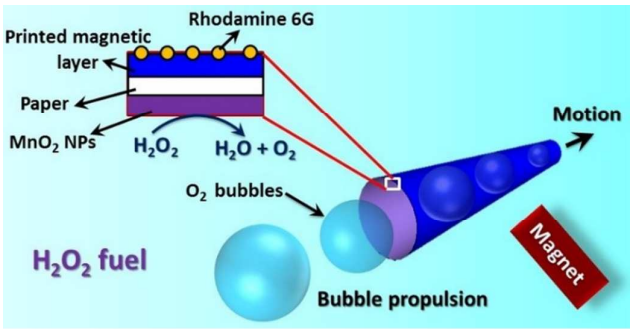

Figure 1. Schematic diagram of the paper-based tubular microjet. The manganese dioxide nanoparticle (MnO_2NP) coated inner wall (lighter violet shade) activated the catalytic decomposition of H_2O_2 to accumulate the O_2 bubbles inside the tubular cavity. The bubbles grew in size along the length of the tube and detached at the end. The issuance of the O_2 bubbles out of the microjets provided the required thrust for motion. The toner ink of printer led to the magnetic layer (darker blue shade), which facilitated magnetic control of the microjet. The payload (Rhodamine 6G) was loaded on the paper microjet.

Figure 1 schematically described the paper based tubular microjet. Initially, the outer side of a flat piece of paper was coated with the toner ink of the printer, which infused the magnetic sensitivity by depositing ferromagnetic layer of Fe_3O_4 microparticles on the paper surface. The deposition of MnO_2NPs in the inner core of paper microjet infused the chemical activation of the paper as the MnO_2NPs could catalytically decompose H_2O_2 into water and produce O_2 bubbles ($2H_2O_2 \rightarrow 2H_2O + O_2$) when the paper was immersed inside a bath of peroxide fuel. Importantly, the MnO_2NPs is regarded as one of the most inexpensive and easily accessible catalysts for H_2O_2 decomposition compared to noble catalytic metals like platinum (Pt). The microjets of size ~ 900 µm with diameter opening of ~350 µm was used for all the experiments reported in the manuscript, unless stated otherwise. The detailed fabrication protocol and characterization of the microjets have been discussed in Supplementary Information (SI). The usage of paper for as base material ensured the biodegradable nature of the microjet. The office waste papers (photocopy, inkjet and laser prints) are in general partially hydrophobic as compared to the filter papers. After the deposition of ferromagnetic printer ink, the office waste papers become more hydrophobic, as experimentally shown in the SI. Thus apart from magnetic sensitivity, the printed layer also protects the microjet from the abrupt aqueous dissolution during catalytic operations inside peroxide fuel to enhance its lifetime.

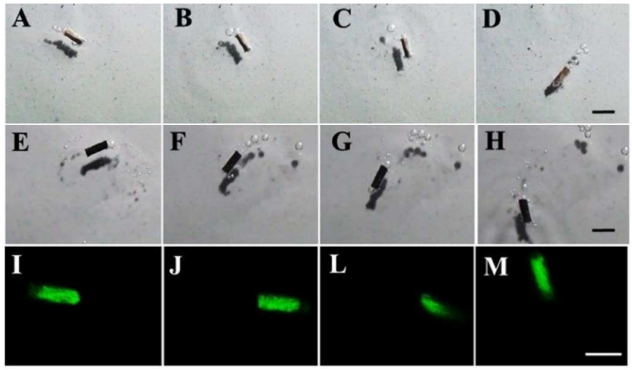

Figure 2. (A-D) shows the motion of a catalytic paper microjet in 16% H_2O_2 fuel, **(E-H)** shows the motion of a magneto-catalytic paper microjet in 16% H_2O_2 fuel in presence of an external magnetic aid, **(I-M)** shows the fluorescent activity of the moving catalytic paper microjet under microscope. The scale bars are of ~900 µm.

Figure 2A-D and Video S1 together show the chemical locomotion of a paper microjet inside a bath of peroxide fuel. When the paper microjet was immersed in 16% (v/v) aqueous peroxide solution, the O_2 bubbles were generated due to the catalytic decomposition of the peroxide fuel on the MnO_2NPs deposited at the inner hollow core of the microjet. The random distribution of the MnO_2NPs on the inner wall of the microjet facilitated asymmetric decomposition of the peroxide fuel. The O_2 gas accumulated as bubbles inside the tubular cavity of the microjet and grew in size due to coalescence. The grown up bubbles periodically advanced towards one of the openings to eject out of the microjet. It may be noted here that we maintained a frustum shape for the tubular jet to have openings with different diameters at the ends, which ensured that most of the O_2 bubbles ejected through the opening with larger diameter. The continuous ejection of the O_2 microbubbles from one side of the microtube provided the thrust for the motion. With the ejection of bubbles from the

opening of larger diameter of the frustum, the MnO_2NPs at the inner core got exposed to fresh peroxide fuel from the other opening of smaller diameter. This led to a periodic ejection of microbubbles from one side to enforce a directed locomotion of the microjet in the opposite direction of the bubble ejection. The microjet migrated with a speed as high as ~2 body lengths per second. The control experiments were performed to confirm the propulsion by O_2 bubbles generated due to catalytic decomposition of H_2O_2 by MnO_2NPs. For example, the **Video S2** showed that the microjet was stationary when was immersed in water (absence of H_2O_2). Further, immersing the uncoated paper microtube in aqueous H_2O_2 failed to produce microbubbles for the propulsion, as shown in the **Video S3**. The mobility of the microjets in 16% (v/v) peroxide fuel accelerated from ~1.6 x 10^{-3} ms^{-1} to ~5 x 10^{-3} ms^{-1} (5.5 body lengths per second) under the coupled influence of chemical activity and external magnetic field of strength 60 mT, as shown in the **Figure 2E-H and Video S4**. The external magnetic control was also beneficial in controlling the direction from the remote location. The motion of the catalytic microjet in aqueous 12% (v/v) H_2O_2 solution could also be monitored under microscope by attaching fluorophore on the outer tube wall, as shown in **Figure 2I-M** and **Video S5**. The fluorescent tracer provided an optical indication of the local position of the motile paper microjet. The experiment confirmed that the trajectory of the microjet can be followed by fluorescence tracking while in locomotion under submerged conditions.

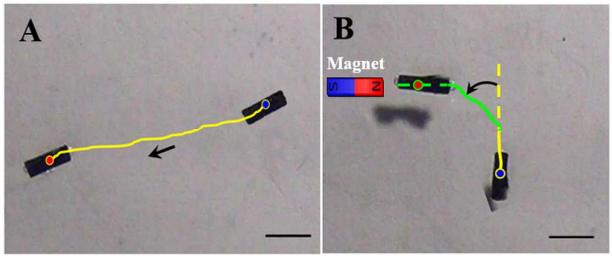

Figure 3. (A) shows the motion of the self-propelling magneto-catalytic paperjet in 10% H_2O_2 fuel.The microjet shows linear self-propulsion in the absence of magnetic field. **(B)** shows the steering of a self-propelling magneto-catalytic paperjet in 10% H_2O_2 fuel. The scale bar is of ~950 µm. The blue and red circles represent the initial and final position of the paperjet, respectively. The yellow line shows the catalytic motion of the microjet and the green shows the magneto-catalytic motion in the presence of magnetic field.

Figure 3A and **Video S6** shows the guided motion of the magneto-catalytic paperjet in 10% (v/v) peroxide solution. The microjet shows self-propulsion in a linear trajectory in the absence of magnetic field, which demonstrates its ability to move along a straight line. Furthermore, the magnetic responsiveness of the magneto-catalytic paperjet was used to veer the self-propelling paperjet (**Figure 3B and Video S7**) in aqueous medium. The microjet was magnetically steered with the help of a bar magnet (0.05 T), which was placed normally to the catalytic-propulsion direction of the microjet. The linearly traversing paperjet was deviated from its path using magnetic field, resulting in the change of its spatial orientation inside the peroxide medium. The microjet showed self-reorientation towards one of the magnetic poles of the magnet and started propelling towards magnetic pole.

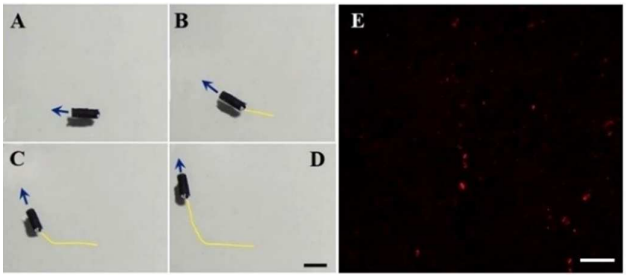

Figure 4. (A-D) shows the controlled motion of a cargo-loaded paper microjet in fuel-free water, in presence of an external magnetic aid. The blue arrow shows the direction of motion and the yellow line shows the motion trajectory. Figures 3A-D show the positions of the motor at t = 0 s, 1 s, 2 s, and 4 s respectively. The scale bar is of ~900 µm. **(E)** The outer magnetic layer of the paper microjet, as observed under microscope at 525 nm excitation wavelength. The red spots depict the localized immobilization of cationic R6G dye. The scale bar is of ~5 µm.

Figure 4A-D and **Video S8** shows the non-catalytic locomotion of a R6G loaded-paper microjet (**Figure 4E**) by using external magnetic field. The directional control over the paper microjet was achieved by varying the position of the localized magnetic field. The external magnet was placed near the paper microjet and the R6G-loaded microjet was veered in desired trajectory. The experiment shows the potential use of miniaturized paper microjets as futuristic biocompatible and fuel-free cargo delivery vector.

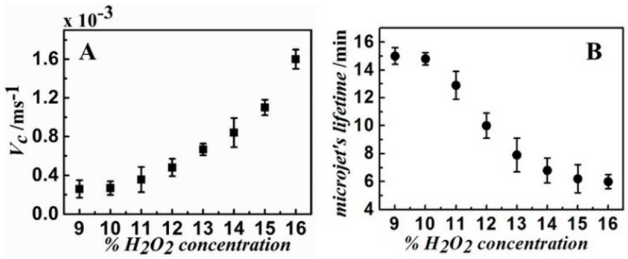

Figure 5. (A) Variation in the average speed (V_c) and **(B)** Lifetime of a ~900 µm paper microjet with increase in concentration of the hydrogen peroxide in the peroxide fuel.

For example, a miniscule version of this microjet prototype loaded with drug payload can not only deliver at the targeted location but also the *in vivo* degradation of paper would facilitate controlled drug release in the acidic environment of the stomach. The increase in H_2O_2 concentration inside the peroxide fuel enhanced the bubble-ejection rate, which in turn raised the velocity of the microjet inside the bath.[33] **Figure 5A** shows that the average speed (V_c) of the microjet increased monotonically with the increase in H_2O_2 concentration (% v/v) inside the peroxide fuel. The plot indicates that the microjet attained the speed of as high as ~1.6 x 10^{-3} ms^{-1} in the 16% (v/v) peroxide fuel (**Video S1**) with a lifespan of ~6 min. The recorded speed was as high as ~2 body lengths per second. In comparison, when the microjet was immersed in a bath of 9% (v/v) peroxide fuel, the speed of the microjet dropped to ~0.27 x 10^{-3} ms^{-1} (**Video S9**) whereas the lifetime increased to ~15 min. The plot clearly shows that the speed of the microjet was a strong function of the concentration of H_2O_2 in the fuel. The velocity profile of the catalytic paper microjet was found to be analogous with previously reported plot by Wang *et al.*[29] for MnO_2 catalytic motor (~5 µm) in 12% -21% peroxide solution.

Furthermore, the experiments also suggested that the higher (lower) peroxide concentration led to a lesser (larger) lifespan for the microjets (**Figure 5B**). The catalytic paper microjets can withstand corrosion of the 9% H_2O_2 for ~15 min due to the partial hydrophobicity of the office waste papers, whereas the usage of 16% H_2O_2 gradually dissolute the paper microjet in ~5 min, thereby reducing its lifetime. The slow dissolution of paper microjets with prolonged time facilitates negligible microjet-accumulation within the system after completion of task.

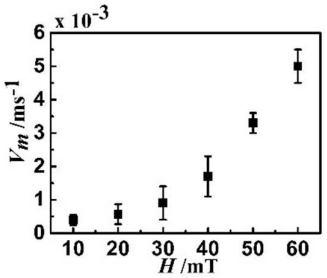

Figure 6. Variation in the average speed (V_m) of a ~ 900 µm magneto-catalytic microjet in 10% (v/v) aqueous H_2O_2 with the increase in the strength of the external magnetic field (H).

The direction and speed of the chemically propelled microjets could be meticulously controlled when the external magnetic field was applied. **Figure 6** shows the variation in the speed (V_m) of microjet towards one of the magnetic poles with the change in the strength of the external magnetic field from 10 mT to 60 mT, while immersed in a bath of 10% (v/v) peroxide fuel. In may be noted here that the microjets were still undergoing the chemical locomotion when the external magnetic field was applied on them. The plot shows that the microjet could migrate with a larger pace when the strength of the external magnetic field was enhanced. The imposed magnetic field induced magnetism to the ferromagnetic coating deposited on the microjet surface, which in turn resulted in an attractive force between the paper microjet and the magnetic pole to stimulate the motion. The paper microjet showed continuous acceleration towards one of the magnetic poles as the magnitude of the magnetic attraction between the particle and the pole increased as the jet progressed towards the pole. Although the increase in the speed was nominal (~0.4 x 10^{-3} ms^{-1}) at a lower magnetic field strength (10 mT), the microjet could move at a speed as high as ~5 x 10^{-3} ms^{-1} (~5.5 body lengths per second) at 60 mT. The plot confirmed that the chemically empowered paper-microjets could remotely be guided as well as speeded up with the help of an external magnetic field. The experiments also suggested that the motor could move even at a faster pace with further increase in the external magnetic field.

4. Conclusions

We report a simple pathway to fabricate paper-based tubular microjets having multimodal chemical and magnetic control over the motion. In contrast to the previously reported fabrication methodologies,[23,34] which not only employed complex multistep processes but also used high end fabrication facilities, the proposed methodology is simple and economic. Importantly, the use of paper as a building block made the microjet biocompatible and biodegradable. The manganese-dioxide nanoparticles at the inner surface of the hollow tubular microjet facilitated the motion by decomposition of hydrogen peroxide when immersed inside a bath of aqueous peroxide fuel. The oxygen bubbles ejecting out of the microjet provided the recoil thrust for the propulsion in a fluidic environment. The speed (lifespan) of the microjet was found to increase (reduce) with the hydrogen peroxide concentration in the peroxide fuel. Attachment of fluorescent tracer helped in tracking the trajectory of the microjet while in motion. The presence of the Fe_3O_4 microparticles on the outer surface of the microtone facilitated the magnetic field induced remote control on the motion. The chemically empowered locomotion of the microjet could be speeded up, slowed down, turned in different directions with the help of the external magnetic control. The proposed paper-based microjets with chemical and magnetic responses have the potential to efficiently meet the challenges related to drug loading and delivery, cell capture,[35] environmental clean-up operations and sensing applications.

Acknowledgements

We thank Sunny Kumar, Divesh Ranjan, and Saptak Rarotra for their help in FTIR and XRD analysis. The support from Central Instrumentation Facility, IIT Guwahati and S. N. Bose National Centre for Basic Sciences, Kolkata for characterization facilities are also gratefully acknowledged. We thank the DST Nano-Mission program, Grant no. SR/NM/NS-1109/2012(G), DeitY - grant no. 5(9)/2012-NANO, and the DST-FIST-grant SR/FST/ETII-028/2010, Government of India, for the financial aids.

Notes and references

A. K. Singh, T. K. Mandal and D. Bandyopadhyay designed all the experiments. A. K. Singh performed the experimental investigations. The manuscript was written through contributions of all authors. All authors have given approval to the final version of the manuscript. The authors declare no conflict of interest.

1 W. F. Paxton, K. C. Kistler, C. C. Olmeda, A. Sen, S. K. St. Angelo, Y. Cao, T. E. Mallouk, P. E. Lammert and V. H. Crespi, *J. Am. Chem. Soc.*, 2004, **126**, 13424–13431.

2 S. Fournier-Bidoz, A. C. Arsenault, I. Manners and G. A. Ozin, *Chem. Commun.,* 2005, **4**, 441–443.

3 S. Sanchez, L. Soler and J. Katuri, *Angew. Chemie Int. Ed.,* 2015, **54**, 1414–1444.

4 M. Xuan, J. Shao, X. Lin, L. Dai and Q. He, *ChemPhysChem*, 2014, **15**, 2255–2260.

5 G. Zhao and M. Pumera, *Nanoscale*, 2014, **6**, 11177–11180.

6 J. Orozco, D. Vilela, G. Valdes-Ramirez, Y. Fedorak, A. Escarpa, R. Vazquez-Duhalt and J. Wang, *Chem. A Eur. J.*, 2014, **20**, 2866–2871.
7 H. Zhang, W. Duan, L. Liu and A. Sen, *J. Am. Chem. Soc.*, 2013, **135**, 15734–15737.
8 J. G. S. Moo and M. Pumera, *Chem. A Eur. J.*, 2015, **21**, 58–72.
9 R. F. Ismagilov, A. Schwartz, N. Bowden and G. M. Whitesides, *Angew. Chemie Int. Ed.*, 2002, **41**, 652–654.
10 Y. S. Song and M. Sitti, *IEEE Trans. Robot.*, 2007, **23**, 578–589.
11 A. A. Solovev, E. J. Smith, C. C. Bufon, S. Sanchez, O. G. Schmidt, *Angew. Chem. Int. Ed.*, 2011, **50**, 10875–10878.
12 W. Wang, L. A. Castro, M. Hoyos and T. E. Mallouk, *ACS Nano*, 2012, **6**, 6122–6132.
13 D. Kagan, M. J. Benchimol, J. C. Claussen, E. Chuluun-Erdene, S. Esener and J. Wang, *Angew. Chemie Int. Ed.*, 2012, **51**, 7519–7522.
14 V. Garcia-Gradilla, J. Orozco, S. Sattayasamitsathit, F. Soto, F. Kuralay, A. Pourazary, A. Katzenberg, W. Gao, Y. Shen and J. Wang, *ACS Nano*, 2013, **7**, 9232–9240.
15 H. R. Jiang, N. Yoshinaga and M. Sano, *Phys. Rev. Lett.*, 2010, **105**, 268302 .
16 L. Baraban, R. Streubel, D. Makarov, L. Han, D. Karnaushenko, O. G. Schmidt and G. Cuniberti, *ACS Nano*, 2013, **7**, 1360–1367.
17 G. Loget and A. Kuhn, *Nat. Commun.*, 2011, **2**, 535.
18 T. R. Kline, W. F. Paxton, T. E. Mallouk and A. Sen, *Angew. Chem.*, 2005, **117**, 754–756.
19 A. A. Solovev, Y. Mei, E. B. Ureña, G. Huang and O. G. Schmidt, *Small*, 2009, **5**, 1688–1692.
20 J. Burdick, R. Laocharoensuk, P. M. Wheat, J. D. Posner and J. Wang, *J. Am. Chem. Soc.*, 2008, **130**, 8164–8165.
21 L. K. E. A. Abdelmohsen, F. Peng, Y. Tu and D. A. Wilson, *J. Mater. Chem. B*, 2014, **2**, 2395–2408.
22 D. Vilela, J. Orozco, G. Cheng, S. Sattayasamitsathit, M. Galarnyk, C. Kan, J. Wang and A. Escarpa, *Lab Chip*, 2014, **14**, 3505–3509.
23 V. Magdanz, M. Guix and O. G. Schmidt, *Robot. Biomimetics*, 2014, **1**, 1–10.
24 Y. Mei, A. A. Solovev, S. Sanchez and O. G. Schmidt, *Chem. Soc. Rev.*, 2011, **40**, 2109–2119.
25 Y. Mei, G. Huang, A. A. Solovev, E. B. Urena, I. Monch, F. Ding, T. Reindl, R. K. Y. Fu, P. K. Chu and O. G. Schmidt, *Adv. Mater.*, 2008, **20**, 4085–4090.
26 A. K. Yetisen, M. S. Akram and C. R. Lowe, *Lab Chip*, 2013, **13**, 2210–2251.
27 M. Ataeefard, *J. Compos. Mater.*, 2014, **0**, 1–9.
28 Y. Wang, X. Zhang, X. He, W. Zhang, X. Zhang and C. Lu, *Carbohydr. Polym.*, 2014, **110**, 302–308.
29 H. Wang, G. Zhao and M. Pumera, *J. Am. Chem. Soc.*, 2014, **136**, 2719–2722.
30 R. Pinto, A. L. Amaral, E. C. Ferreira, M. Mota, M. Vilanova, K. Ruel and M. Gama, *BMC Biotechnol.*, 2008, **8**, 1–7.
31 A. K. Singh, K. K. Dey, A. Chattopadhyay, T. K. Mandal and D. Bandyopadhyay, *Nanoscale*, 2014, **6**, 1398–1405.
32 S. F. DeLauder and D. A. Kidwell, *Forensic Sci. Int.*, 2000, **107**, 93–104.
33 J. Li, G. Huang, M. Ye, M. Li, R. Liu and Y. Mei, *Nanoscale*, 2011, **3**, 5083–5089.
34 J. C. Claussen, M. A. Daniele, J. Geder, M. Pruessner, A. J. Ma, B. J. Melde, M. Twigg, J. M. Verbarg and I. L. Medintz, *ACS Appl. Mater. Interfaces*, 2014, **6**, 17837.
35 S. Campuzano, J. Orozco, D. Kagan, M. Guix, W. Gao, S. Sattayasamitsathit, J. C. Claussen, A. Merkoci and J. Wang, *Nano Lett.*, 2012, **12**, 396–401.